On the Shock-Capturing Properties of a Pressure-Based Method for the Simulation of Compressible Flows

By M. Boger, X. Y. Hu† and C.-D. Munz

Institut für Aerodynamik und Gasdynamik, Universität Stuttgart
Pfaffenwaldring 21, 70569 Stuttgart

A pressure-based scheme for the simulation of compressible as well as incompressible flows is presented and assessed with the help of several one-dimensional test cases. The scheme is used in a conservative formulation. In this context, the energy equation is reformulated in terms of pressure and kinetic energy establishing the pressure-based character of the approach. The method is able to handle compressible flows as accurate results are obtained for standard one-dimensional shock tube test cases. In this contribution, we investigate the shock-capturing property of our pressure-based approach and compare it to a density-based Godunov-type finite volume scheme. Both approaches are applied to Riemann problems characterized by large initial density jumps and to a slowly moving shock wave. From the literature, both cases are known to be critical for Godunov-type schemes. In direct comparison to the density-based finite volume scheme, the pressure-based method reveals to have inferior shock-capturing properties in the case of large density jumps, while the simulation results for slowly moving shocks are superior to those of the Godunov-type finite volume method which indicates tendencies to generate spurious oscillations.

1. Introduction

In the field of computational fluid dynamics there are two well-established concepts of flow simulation algorithms that are called pressure- and density-based methods. While pressure-based approaches are widely used to simulate hydrodynamic flows on the basis of the incompressible flow equations, the density-based schemes can be considered to be the standard methods for compressible flows. Both approaches are distinguished by the use of pressure and density as primary variable, respectively. Although the requirements for the simulation of compressible and incompressible flows differ considerably, a lot of effort has been put into efficiently accessing the weakly compressible regime with both methods. For this purpose, so-called preconditioning techniques are used e.g. for the density-based approaches. On the other hand, the originally pressure-based methods can also be extended to the compressible flow regime.

However, the transition from incompressible to compressible flow is subtle. The underlying equations require different numerical approaches as their mathematical properties change. While inviscid compressible flows are described by a set of hyperbolic equations, their incompressible counterpart is of hyperbolic-elliptic nature. One possibility

† Lehrstuhl für Aerodynamik und Strömungsmechanik, Technische Universität München, Boltzmannstr. 15, 85748 Garching b. München

for extending a pressure-based incompressible algorithm to the compressible regime is the so-called multiple pressure variables (MPV) approach proposed by Munz *et al.* [1,2]. The method builds upon a pressure decomposition in dependency of a global flow Mach number. In this context, the conservative energy equation is reformulated in terms of pressure and kinetic energy. Therefore, the total energy is first split in its internal and kinetic part. Afterwards, the internal energy is replaced with the help of an equation of state (EOS). Finally, the numerical algorithm includes the solution of a pressure Poisson equation, similar to classical incompressible schemes.

In the following we apply the MPV method and a standard Godunov-type scheme to different one-dimensional shock-tube test cases in order to assess their shock-capturing properties. Especially shock tube problems with large density jumps pose problems to all numerical schemes, including the density-based Godunov-type methods, which is known from the literature [3, 4]. Moreover, several other defects of numerical schemes exist that are related to the solution of a Riemann problem [5]. Here, we focus on the slowly moving shock of Quirk [5] as a second test problem. A very detailed analysis of this phenomenon can be found in [6]. In both cases, the properties of the MPV scheme have been investigated in a detailed way and directly compared to a standard density-based finite volume solver.

The outline of the paper is as follows. In the first section, the governing equations for the numerical simulation are introduced. This is followed by the introduction of the basic notions of the MPV approach. In the following section, the results of the shock-capturing investigation for the pressure-based MPV and the density-based finite volume solver are presented and discussed.

2. Governing equations

In this section we describe the equations that are used for the numerical simulations with the pressure-based method.

2.1. *Compressible Euler equations*

The conservation equations for mass, momentum and total energy for inviscid flows without gravitational and external forces and heat conduction in compressible gas dynamics are given by the Euler equations

$$\frac{\partial \rho}{\partial t} + \nabla \cdot (\rho \mathbf{v}) = 0 \,, \tag{2.1}$$

$$\frac{\partial (\rho \mathbf{v})}{\partial t} + \nabla \cdot [(\rho \mathbf{v}) \circ \mathbf{v}] + \frac{1}{M^2} \nabla p = 0 \,, \tag{2.2}$$

$$\frac{\partial e}{\partial t} + \nabla \cdot [(e + p) \mathbf{v}] = 0 \,. \tag{2.3}$$

Here, a non-dimensional formulation is used where ρ denotes the density, p the pressure, $\mathbf{v}$ the velocity and e the total energy per unit volume. In order to be able to consider the Euler equations in their incompressible limit, a parameter called global flow Mach number M is introduced in the above equations. The global flow Mach number results from the choice of different reference values for the speed of sound and the fluid velocity

$$M = \frac{|\mathbf{v}_{ref}|}{\sqrt{p_{ref}/\rho_{ref}}} \,. \tag{2.4}$$

The system (2.1)-(2.3) has to be closed with an EOS relating the pressure to the known flow variables. In the following, the ideal gas EOS is used in a dimensionless formulation including the above global flow Mach number parameter M

$$p = (\gamma - 1)(e - M^2 \frac{\rho}{2} |\mathbf{v}|^2). \tag{2.5}$$

3. Pressure-based flow solver

The non-dimensional Euler equations (2.1)-(2.3) are solved by the pressure-based MPV scheme in conservative formulation [2]. It is capable to handle the case of compressible flows ($M = 1$) as well as the incompressible limit ($M = 0$).

3.1. *The multiple pressure variables (MPV) approach*

The vanishing global Mach number $M = 0$ poses a severe problem: the momentum equation (2.2) shows a singular behavior because of the factor $1/M^2$. The Euler equations change their type from hyperbolic to hyperbolic-elliptic in the incompressible case. In order to circumvent this singularity the MPV scheme is based on an asymptotic expansion of the pressure in terms of the global flow Mach number M

$$p(x, t) = p^{(0)}(t) + M^2 p^{(2)}(x, t). \tag{3.1}$$

The leading order pressure term $p^{(0)}$ satisfies the EOS in the limit case $M = 0$ and it is therefore called thermodynamic background pressure. The pressure $p^{(2)}$ can be considered to be a hydrodynamic pressure as it guarantees the divergence-free condition for incompressible flows at $M = 0$. Due to the pressure splitting, the term $1/M^2 \nabla p$ in Eq. (2.2) remains bounded in the incompressible limit and reduces to $\nabla p^{(2)}$. Hence, this pressure decomposition takes into account the different roles of pressure for compressible and incompressible flows.

Inserting the ideal gas EOS (2.5) and the pressure decomposition (3.1) into the non-dimensional Euler equations (2.1)-(2.3) we arrive at the following system

$$\begin{pmatrix} \rho \\ \rho\mathbf{v} \\ p + (\gamma - 1)M^2 e_k \end{pmatrix}_t + \nabla \cdot \begin{pmatrix} \rho\mathbf{v} \\ (\rho\mathbf{v}) \circ \mathbf{v} \\ (\gamma - 1)M^2 e_k \mathbf{v} \end{pmatrix}^{ex}$$
$$+ \nabla \cdot \begin{pmatrix} 0 \\ p^{(2)}\mathbf{I} \\ \gamma p\mathbf{v} \end{pmatrix}^{im} = \begin{pmatrix} 0 \\ 0 \\ 0 \end{pmatrix}. \tag{3.2}$$

Here, $\mathbf{I}$ designates the unity matrix. The most obvious change is apparent in the energy equation that is now expressed in a pressure formulation such that the MPV method uses the pressure as primary variable instead of the energy. The Euler equations are still in conservative formulation and the MPV approach builds upon a semi-implicit time discretization. This is visible from the superscripts ex and im that designate the explicit and implicit time discretization of the respective terms. In this context, convective terms are treated in an explicit manner while all terms linked to the speed of sound are discretized implicitly. The spatial discretization is carried out on a Cartesian staggered grid, avoiding the decoupling of pressure and velocity in the incompressible limit case. The explicit flux terms are discretized in an upwind manner, while for the implicit part a central difference discretization is used. A more detailed description of the numerical method can be found in [2].

4. Shock-capturing properties of the MPV method

In the course of this section, the MPV scheme is applied to several shock tube test cases characterized by an increasing initial density jump in order to test its shock-capturing properties. Furthermore, the behavior of the numerical scheme with respect to a slowly moving shock is investigated. In both cases, the results of the MPV approach are compared to those obtained with a standard Godunov-type density-based finite volume scheme.

4.1. *Strong rarefactions*

In a first step, the MPV scheme is used to solve several shock tube problems. Our investigations are mainly based on the work of Kudriakov *et al.* [4] that identified strong rarefaction waves to be the origin of bad shock-capturing behavior. According to their definition, a strong rarefaction is identified by a large difference in speed of the head and the tail wave of the rarefaction fan that can be measured by the relation r of the wave slopes m

$$r = \left| \frac{m_{Head}}{m_{Tail}} \right| \tag{4.1}$$

Following the reasoning of [4], the ratio r can be considered to be critical for $r > 10$ and the shock-capturing errors can be explained as follows.

At every time step, an averaging error is introduced at the vicinity of the contact discontinuity. As the boundaries of the rarefaction fan are traveling at very different speeds, the slow tail wave is supposed to stay close to the contact discontinuity for many time steps. Therefore, from the beginning of the computation, the averaging errors accumulate in this region which finally leads to the mispredicted shock wave.

In order to characterize our pressure-based approach, we apply it to a series of shock tube problems with increasing initial density jumps, thus successively raising the rarefaction strength. We measure the strength by the proposed wave speed ratio r and additionally compare the numerical results to those of a standard density-based finite volume solver. Both numerical schemes use a discretization of first order in time and space and the number of grid cells is equal, too. The finite volume solver CFDFV is of Godunov-type and several Riemann solvers are available for the intercell flux calculation. In the following, an exact Riemann solver is employed unless otherwise stated.

The basis for the test series is the standard Sod test case, according to [7]

$$\begin{pmatrix} \rho_L \\ v_L \\ p_L \\ \gamma_L \end{pmatrix} = \begin{pmatrix} 1.0 \\ 0 \\ 1 \\ 1.4 \end{pmatrix} ; x < 0.5 \qquad \begin{pmatrix} \rho_R \\ v_R \\ p_R \\ \gamma_R \end{pmatrix} = \begin{pmatrix} 0.125 \\ 0 \\ 0.1 \\ 1.4 \end{pmatrix} ; x > 0.5. \tag{4.2}$$

The corresponding results of the schemes, obtained with 100 grid cells, are displayed in Fig. 1. In general, both solvers approximate the exact solution quite well as the strength and the position of all waves are correctly predicted. Yet a closer look at the velocity plot reveals that the result of the MPV method differ a bit stronger from the exact solution of the rarefaction than those of the finite volume solver.

The indicator r shows a moderate wave speed ratio

$$r = \left| \frac{m_{Head}}{m_{Tail}} \right| = 2.78. \tag{4.3}$$

In a second step, the initial discontinuity in density is now increased by a factor of 10,
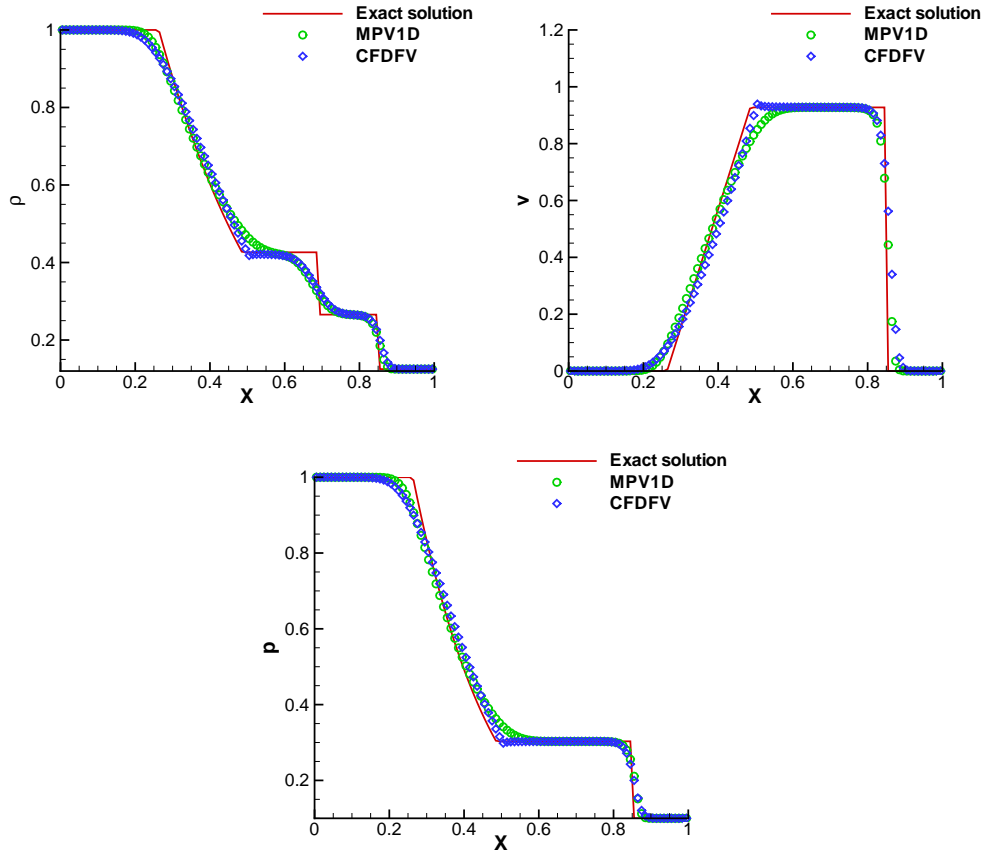
FIGURE 1. Sod test: density, velocity and pressure plot of the MPV and the finite volume CFDFV simulation (first order, 100 grid cells) and the exact solution at $t = 0.2$.

augmenting the density ρ_L

$$\begin{pmatrix} \rho_L \\ v_L \\ p_L \\ \gamma_L \end{pmatrix} = \begin{pmatrix} 10.0 \\ 0 \\ 1 \\ 1.4 \end{pmatrix} ; x < 0.5 \qquad \begin{pmatrix} \rho_R \\ v_R \\ p_R \\ \gamma_R \end{pmatrix} = \begin{pmatrix} 0.125 \\ 0 \\ 0.1 \\ 1.4 \end{pmatrix} ; x > 0.5. \qquad (4.4)$$

Due to the raise in the density ratio, the rarefaction wave speed ratio is increased to

$$r = \left| \frac{m_{Head}}{m_{Tail}} \right| = 4.57. \qquad (4.5)$$

Since this problem is already more severe compared to the previous one, the spatial resolution has been increased by using 300 grid cells to discretize the domain. Both solvers are applied to the modified test case (4.4) and the results can be found in Fig. 2.

The numerical solution of both schemes is close to the exact one. Again, the MPV approach is inferior to the finite volume approach with respect to the resolution of the
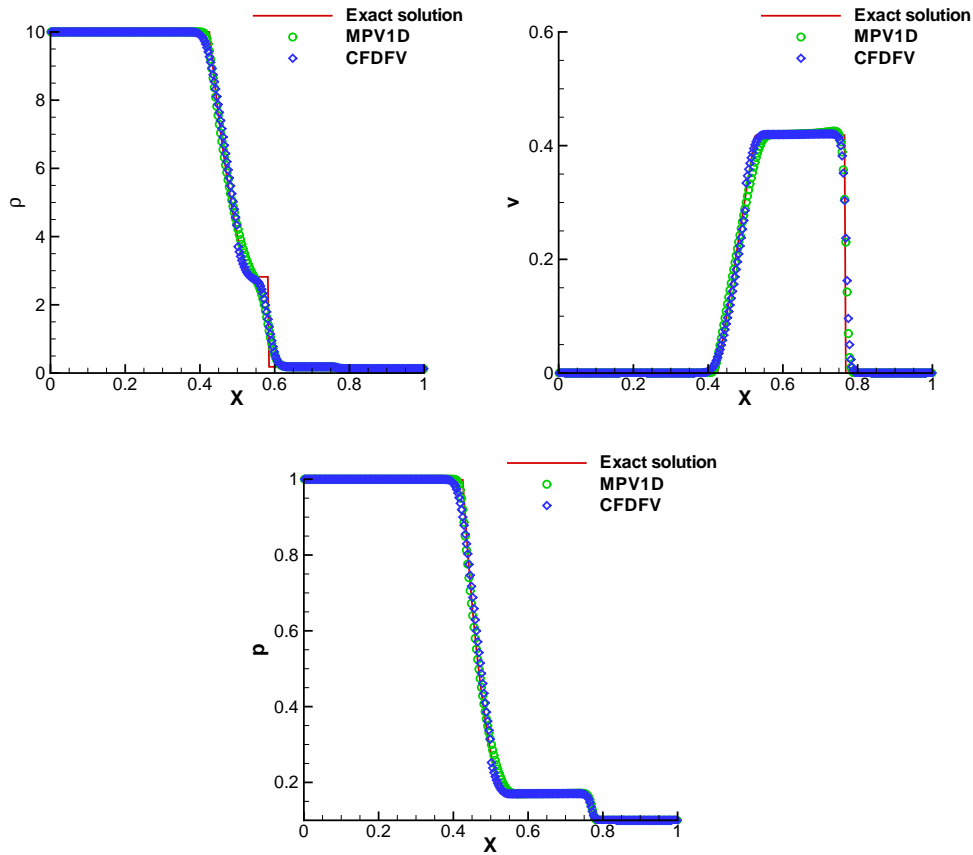
FIGURE 2. Modified Sod test (density ratio $\rho_L/\rho_R = 80$): density, velocity and pressure plot of the MPV and the finite volume CFDFV simulation (first order, 300 grid cells) and the exact solution at $t = 0.2$.

expansion fan. Furthermore, the pressure-based method produces a small overshoot at the shock position that is visible in the velocity plot.

Finally, an even more demanding test is performed by further increasing the density ρ_L to $\rho_L = 100$, leading to a ratio of $\rho_L/\rho_R = 800$

$$\begin{pmatrix}\rho_L \\ v_L \\ p_L \\ \gamma_L\end{pmatrix} = \begin{pmatrix}100.0 \\ 0 \\ 1 \\ 1.4\end{pmatrix}; x < 0.5 \qquad \begin{pmatrix}\rho_R \\ v_R \\ p_R \\ \gamma_R\end{pmatrix} = \begin{pmatrix}0.125 \\ 0 \\ 0.1 \\ 1.4\end{pmatrix}; x > 0.5. \qquad (4.6)$$

Hereby, the indicator r further raises to

$$r = \left|\frac{m_{Head}}{m_{Tail}}\right| = 6.06. \qquad (4.7)$$

The outcome of the computations is shown in Fig. 3. This time, the MPV method clearly has trouble to capture the shock since neither its position nor its strength are predicted accurately, as it is obvious from the velocity plot. While the finite volume scheme gives
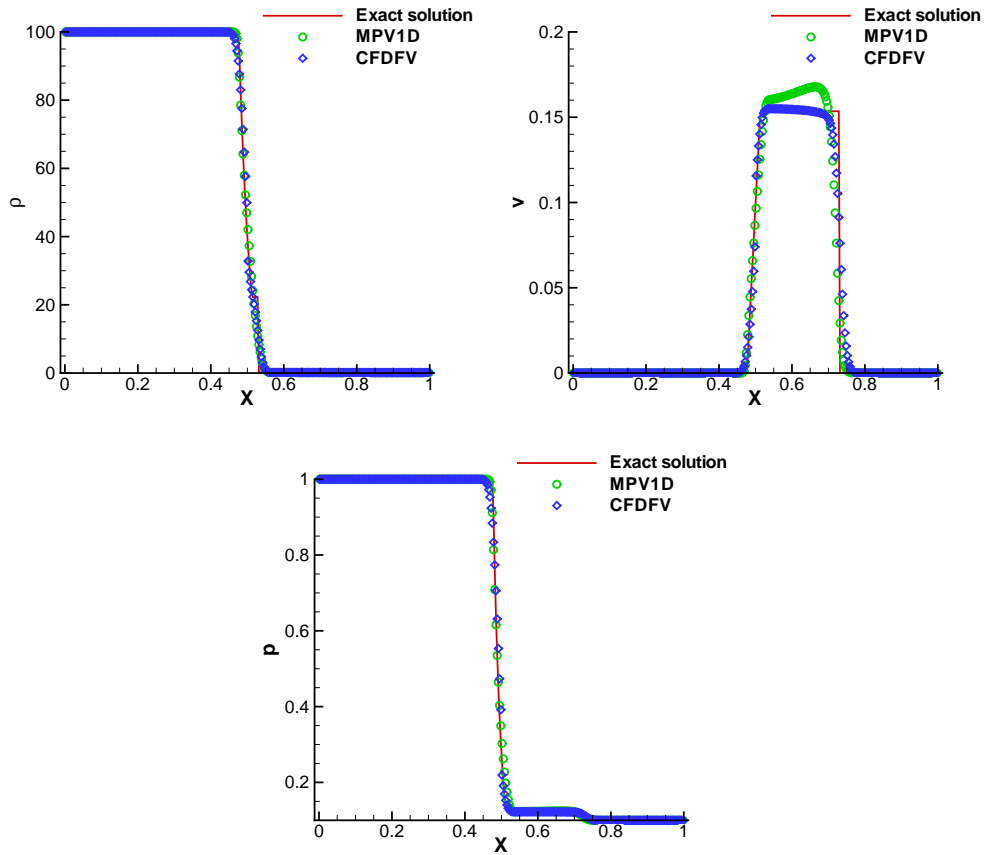
FIGURE 3. Modified Sod test (density ratio $\rho_L/\rho_R = 800$): density, velocity and pressure plot of the MPV and the finite volume CFDFV simulation (first order, 300 grid cells) and the exact solution at $t = 0.2$.

the same incorrect shock position it still resolves the correct strength of the shock, hence showing a better result.

This displays the inferiority in shock-capturing of the pressure-based MPV method in comparison to a standard finite volume scheme in the presence of large density ratios. To further investigate and confirm this observation, the difference in wave speeds in the rarefaction is drastically increased by not only imposing a high initial density ratio but also having a considerable jump in pressure

$$\begin{pmatrix} \rho_L \\ v_L \\ p_L \\ \gamma_L \end{pmatrix} = \begin{pmatrix} 1.0376 \\ 6.0151 \\ 1000 \\ 1.4 \end{pmatrix} ; x < 0.7 \qquad \begin{pmatrix} \rho_R \\ v_R \\ p_R \\ \gamma_R \end{pmatrix} = \begin{pmatrix} 0.001 \\ 0 \\ 1 \\ 1.4 \end{pmatrix} ; x > 0.7. \qquad (4.8)$$

In this case pressure and density have an initial ratio of about 1000.

So far, the shock-capturing problem has always been most obvious in the velocity and therefore Fig. 4 illustrates the corresponding results of the MPV scheme and the finite
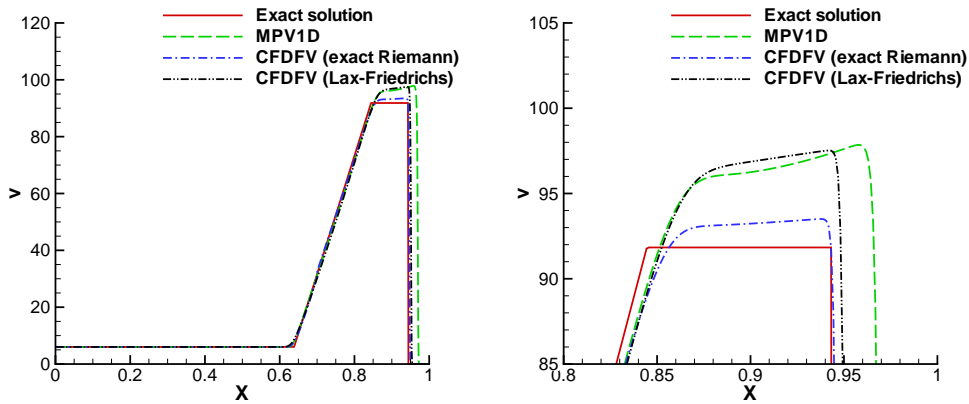
FIGURE 4. Severe shock tube case (density ratio $\rho_L/\rho_R = 1037.6$, pressure ratio $p_L/p_R = 1000$): velocity plot (left) and close-up (right) of the MPV and the finite volume CFDFV simulation (first order, 800 grid cells) and the exact solution at $t = 0.002$.

volume solver for this test. From the plot on the left, it is already clearly visible that the MPV scheme is considerably deviating from the exact solution.

The finite volume scheme is used with two different flux calculation approaches, an exact Riemann solver and the Lax-Friedrichs method. While the exact Riemann solver is the most accurate way of flux evaluation, the Lax-Friedrichs flux represents a quite simple approximation to the solution of the exact Riemann problem. Thus, the quality of flux evaluation is considerably varied by the use of the two methods.

For this severe test, even the finite volume scheme is unable to accurately capture the shock. The plot on the right side is a close-up on the shock location. While the finite volume solver has problems in resolving the strength correctly, it still catches the position of the shock quite acceptably using the exact Riemann solver for the numerical flux evaluation. However, the shock is completely mispredicted by the MPV method. When the flux calculation method in the finite volume scheme is changed to the less accurate Lax-Friedrichs flux, the results are tending towards those of the MPV code. This indicates a strong dependency on the quality of the flux calculation.

According to [4], the main difficulty for numerical schemes in dealing with strong rarefactions is to minimize the averaging errors over the rarefaction fan at the beginning of the computation. If the numerical scheme has problems to correctly build up the wave pattern, the solution inevitably stays disturbed for the rest of the calculation. This effect can be demonstrated by a test, where the initial solution is not a discontinuity, but the exact solution of the shock tube problem (4.8) at the instance $t = 5 \cdot 10^{-4}$. For this setup, the velocity plot of the MPV scheme is displayed in Fig. 5. Starting from the developed wave structure, the MPV method is able to further evolve the waves correctly as strength and position of the shock coincide with the exact solution. This illustrates the problems of the pressure-based method to capture the right waves from an initial discontinuity due to the lack of an accurate Riemann solver. Being faced with an initial discontinuity, the waves develop over several time steps during which the problem is not fully resolved on the computational mesh and physical behavior has to be ensured via the numerical flux calculation.

In this context, a strong dependency on the quality of the numerical flux can be de-
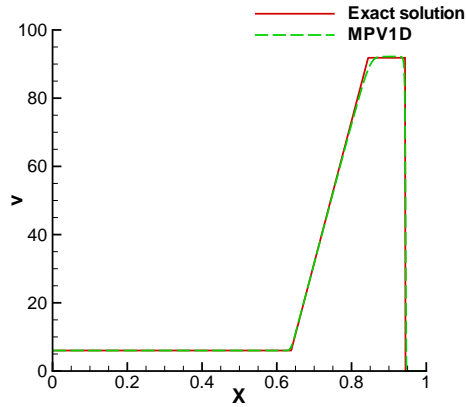
FIGURE 5. Severe shock tube case (density ratio $\rho_L/\rho_R = 1037.6$, pressure ratio $p_L/p_R = 1000$). The problem is initialized using the exact solution at $t = 5 \cdot 10^{-4}$ that already contains the fully developed wave pattern: velocity plot of the MPV simulation (first order, 800 grid cells) and the exact solution at $t = 0.002$.

duced. While the finite volume scheme with the exact Riemann solver performs soundly, the results are remarkably deteriorating when the flux evaluation is changed to the less accurate Lax-Friedrichs flux (cf. Fig. 4). The MPV method uses an upwind method in combination with a central difference discretization for the implicit part. Obviously, this discretization approach further degrades the numerical results in direct comparison to the finite volume approach with the already quite inaccurate Lax-Friedrichs flux. Moreover, the results of Fig. 5 indicate that the numerical flux is most important in the beginning of the computation to set up the wave pattern, as the MPV scheme is capable of correctly evolving the shock in time starting from the already existing waves.

4.2. *Slowly moving shock*

As a second example, the movement of a slow shock is investigated with the two numerical schemes. Following [5] a shock wave is simulated that is slowly moving from left to right. The pre- and post-shock states are given by the following initial conditions

$$
\begin{pmatrix} \rho_L \\ v_L \\ p_L \\ \gamma_L \end{pmatrix} = \begin{pmatrix} 3.86 \\ -0.81 \\ 10.33 \\ 1.4 \end{pmatrix} ; x < 0.5 \qquad \begin{pmatrix} \rho_R \\ v_R \\ p_R \\ \gamma_R \end{pmatrix} = \begin{pmatrix} 1.0 \\ -3.44 \\ 1.0 \\ 1.4 \end{pmatrix} ; x > 0.5. \tag{4.9}
$$

The MPV and the density-based finite volume solver have been applied to the above initial conditions and the corresponding results are displayed in Figs. 6-8. For the test, the first order version of both solvers was used on a grid consisting of 100 cells and the simulation was stopped at $t = 1.75$.

A first look at the density plot of Fig. 6 already reveals the presence of oscillations behind the right moving shock for the finite volume solver. The plot on the right is a close-up view at the post-shock area. Here, the oscillations of the density-based scheme are clearly visible while the solution of the pressure-based method is free of oscillations. The same is true for the velocity and pressure distributions in Fig. 7 and Fig. 8. In all cases, the post-shock solution of the finite volume solver is characterized by pronounced oscillations.
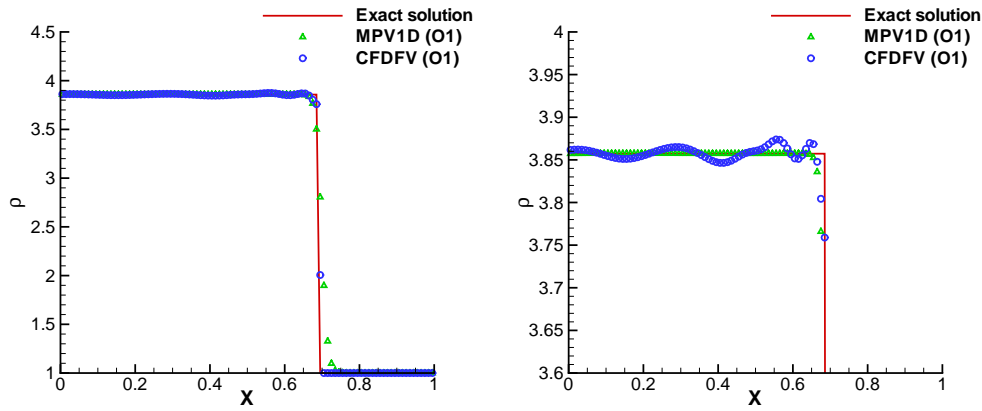
FIGURE 6. Solution of the slowly moving shock (4.9): density plot of the MPV and the finite volume CFDFV simulation at the time $t = 1.75$, including close-up view at the right (first order, 100 grid cells). The CFDFV code was used with an exact Riemann solver.
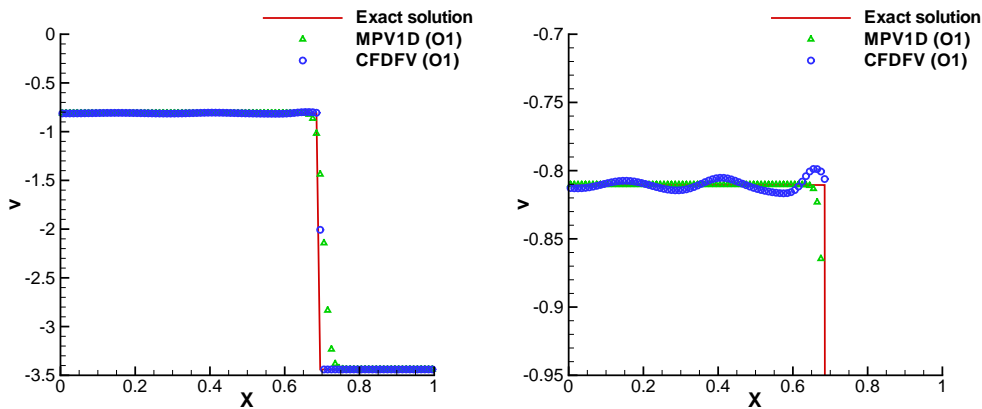

FIGURE 7. Solution of the slowly moving shock (4.9): velocity plot of the MPV and the finite volume CFDFV simulation at the time $t = 1.75$, including close-up view at the right (first order, 100 grid cells). The CFDFV code was used with an exact Riemann solver.

With reference to [5] the resolution of a slowly moving shock is a well known defect of all Godunov-type schemes that can be explained by the fact that they build on the recognition of wave patterns. Hence, spurious waves are introduced connecting the pre- with the post-shock state that are not present in the physical problem consisting of a single shock wave.

Yet, the pressure-based scheme is not trying to identify certain waves, as it is based on upwind formulae and a central difference discretization. Therefore, the corresponding results are free of oscillations and superior to those of the density-based Godunov-type schemes.
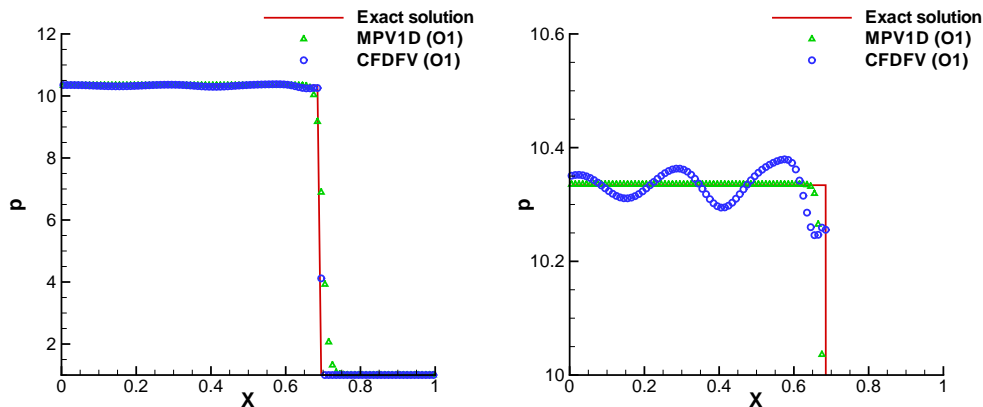
FIGURE 8. Solution of the slowly moving shock (4.9): pressure plot of the MPV and the finite volume CFDFV simulation at the time $t = 1.75$, including close-up view at the right (first order, 100 grid cells). The CFDFV code was used with an exact Riemann solver.

5. Conclusion

The pressure-based MPV method for the computation of compressible as well as incompressible flows has been presented. In the present contribution, the scheme was applied to several Riemann problems known to be critical for standard flow solvers, in order to assess its shock-capturing properties.

On the one hand, several shock tube tests have been performed and compared to the results of a standard Godunov-type finite volume solver. According to the findings of Kudriakov *et al.* [4], both methods run into trouble when they have to deal with large initial density ratios, but the shock-capturing properties of the pressure-based method reveal to be inferior to those of the finite volume scheme. The issue appears to be related to the accuracy of the numerical flux evaluation that plays a crucial role for these kind of Riemann problems. Changing the numerical flux calculation of the finite volume scheme directly leads to a change in the predicted shock position and strength. Since the flux calculation for the semi-implicit pressure-based method cannot be changed as easily as for the explicit finite volume scheme, the accurate resolution of strong rarefactions seems to be a problem for the pressure-based MPV approach.

On the other hand, the absence of an explicit Riemann solver has proven to be an advantage in the case of the slowly moving shock wave of Quirk [5]. There, the fact that the wave structures are not explicitly resolved by the numerical scheme prevents the results from being oscillatory.

Acknowledgments

References

[1] Munz, C.-D., Roller, S., Klein, R., Geratz, K. J. and Reitz, R. D. (2003). The extension of incompressible flow solvers to the weakly compressible regime. *Computers & Fluids*, **32**(2), 173–196.

[2] Park, J. H. and Munz, C.-D. (2005). Multiple pressure variables methods for fluid flow at all Mach numbers. *International Journal for Numerical Methods in Fluids*, **49**, 905–931.

[3] Tang, H. and Liu, T. (2006). A note on the conservative schemes for the Euler equations. *Journal of Computational Physics*, **218**, 451–459.

[4] Kudriakov, S. and Hui, W. H. (2007). On a new defect of shock-capturing methods. *Journal of Computational Physics*, **227**, 2105–2117.

[5] Quirk, J. J. (1994). A contribution to the great Riemann solver debate. *International Journal for Numerical Methods in Fluids*, **18**, 555–574.

[6] Roberts, T. W. (1990). The Behavior of Flux Difference Splitting Schemes near Slowly Moving Shock Waves. *Journal of Computational Physics*, **90**, 141–160.

[7] Toro, E. F. (1999). *Riemann Solvers and Numerical Methods for Fluid Dynamics*. Springer.